Liquid Crystals
Publication details, including instructions for authors and subscription information:
http://www.informaworld.com/smpp/title~content=t713926090

Frequency variation of periodic distortion thresholds in a nematic liquid crystal

Shila Garg; Steven Wild; Ben Zurn Salman Saeed; U. D. Kini

Online publication date: 06 August 2010

To cite this Article Garg, Shila , Wild, Steven , Saeed, Ben Zurn Salman and Kini, U. D.(1998) 'Frequency variation of periodic distortion thresholds in a nematic liquid crystal', Liquid Crystals, 24: 4, 501 — 517
To link to this Article: DOI: 10.1080/026782998206957
URL: http://dx.doi.org/10.1080/026782998206957

LIQUID CRYSTALS, 1998, VOL. 24, NO. 4, 501–517

Frequency variation of periodic distortion thresholds in a nematic liquid crystal

by SHILA GARG*, STEVEN WILD†, BEN ZURN‡, SALMAN SAEED§
Department of Physics, College of Wooster, Wooster, Ohio 44691, USA

and U. D. KINI
Raman Research Institute, Bangalore 560 080, India

(*Received 12 September 1997; accepted 28 October 1997*)

Investigations are reported on the electric field induced orientational transitions in the bend Fréedericksz geometry under the action of a stabilizing magnetic field. When the magnetic field is strong enough, the deformation above electric threshold is periodic with the periodicity disappearing at a higher voltage. The alignment does not remain homeotropic below threshold and the sample exhibits pretransitional biaxiality. Every transition is discontinuous and accompanied by hysteresis. The expected form of scaling appears to hold for all the observed thresholds. The thresholds and the direction of the wave vector are frequency dependent, showing that the instability mechanism involves electrical conductivity.

1. Introduction

The application of external electric (**E**) and magnetic (**H**) fields along suitable directions in nematic liquid crystals leads to a number of interesting effects, many of which are well accounted for in terms of the continuum theory [1, 2]. These effects arise when the destabilizing orienting torques due to external fields overcome stabilizing elastic torques. The orientation of a well-aligned nematic sample (see ref. [3] for reviews on interfacial properties) becomes stabilized by the application of **H** along **n** if the diamagnetic anisotropy is positive ($\chi_A > 0$). If **H** is impressed on the aligned sample normal to the initial orientation, a homogeneous deformation (HD) results, with **n** uniformly distorted in the sample plane, provided that **H** exceeds the Fréedericksz threshold. In materials with high elastic anisotropy [4, 5], the deformation above the magnetic threshold is striped or periodic (PD). The occurence of PD in these cases has been explained by the use of continuum theory [4, 6].

Static deformations under the action of **E** are also possible but their theoretical interpretation is more involved than in the case of **H** due to the presence of flexoelectricity [7] as well as to the importance of the modification of **E** inside the nematic sample caused by director gradients [8, 9]. A variety of effects arises depending upon various factors, such as the frequency (f) of applied voltage, the initial alignment, presence of ionic impurities, signs of dielectric anisotropy (ε_A) and electrical conductivity anisotropy (σ_A), sample thickness and magnitudes of viscoelastic constants [2]. One of the widely studied nematics is MBBA with $\varepsilon_A < 0$ and $\sigma_A > 0$. In sufficiently pure planar aligned samples of such a material, a static PD [10] can manifest itself due to flexoelectricity [7] under the action of a d.c. field applied normal to the sample plane. If the sample contains ionic impurities, a variety of electrohydrodynamic instabilities (EHDI) can be observed culminating in 'dynamic scattering' at high voltages [2]. The simplest of these instabilities is seen as 'Williams domains' which appear as a static stripe pattern caused by uniform cellular flow inside the sample. The 'Carr–Helfrich mechanism' provides an explanation for the appearance of these roll patterns [11]. The electric threshold is a strong function of f [12]; variations of f and voltage also lead to the observation of a number of instability modes [13] akin to the 'cascade of instabilities' observed in isotropic liquids. Other mechanisms such as charge injection, are also known to become important in many cases [2]. A number of studies have been reported [14] on the simultaneous action of **E** and **H** fields on nematic samples of various dimensions; dynamic scattering, material flow and formation of defects have been investigated.

*Author for correspondence.
†Present address: Physics Department, Indiana University, IN, USA.
‡Present address: Mechanical Engineering Department, University of Minnesota, MN, USA.
§Present address: Liquid Crystal Institute, Kent State University, OH, USA.

Studies on homeotropically aligned positive ε_A materials like 5CB [15] have been reported with the alignment stabilized by **H** applied normal to the plates and destabilized by an a.c. **E** field along the sample plane [16–17]. Under the joint actions of **H** and **E**, a number of interesting deformations result. In thick samples the transition occurring with increasing voltage is discontinuous [16] as predicted earlier [18], but the hysteresis width is much less than that expected theoretically. The transition is preceded by field induced biaxiality [17] similar to that observed in other geometries [19]. The deformation above the transition is periodic and appears to involve no hydrodynamic flow [16]. Attempts have been made [20, 21] to explain the occurrence of PD in refs [16, 17] as a purely dielectric effect.

Investigations with thin samples and electrodes of circular cross-section [22] reveal a marked dependence of the nature of the striped pattern on sample thickness; an attempt has been made to qualitatively interpret the deformation in terms of both dielectric and conductive properties of the material. Subsequent work on thick samples [23] shows that the direction of periodicity of PD depends on the stabilizing magnetic strength. There also exists clear evidence of field inhomogeneities inside the medium caused by the electrode shape. Recent studies on 5CB have indicated [24] that thresholds as well as the direction of periodicity of PD depend on f. At high f (1 KHz), PD forms only in the presence of a sufficiently strong **H** when the voltage is increased from zero. Increase of voltage causes successive transition with change in the periodicity wavevector of PD. At high voltage, the sample becomes aligned and stripe-free. Under d.c. excitation or at low f (5 Hz), convective hydrodynamic flow (EHDI) is observed; at sufficiently elevated voltage, the flow even turns turbulent. This establishes the involvement of electrical conductivity in the formation of PD. Exact theoretical modelling of these phenomena is difficult without a more detailed empirical understanding of the parameters connected with PD.

Some questions also require answers. The detection of PD can be effected visually or by measuring the output from a photodiode. Do both methods lead to the same value for the observed PD threshold? The first transition from the initial homeotropic state is accompanied by field induced biaxiality. How does the extent of this biaxiality depend on different parameters? At a given f, PD has a lower cutoff **H** field. How does the cutoff vary with f? Almost every transition is known to be discontinuous and hysteretic. How does the hysteresis width depend on H and f? Thresholds of static deformations are known to obey approximately certain scaling laws. Do scaling laws exists for the PD thresholds? The experiments are conveniently performed only with voltages that are stepped up at a low rate. It is well known [25] that the sudden application of a destabilizing field can lead to transient periodic structures. Is PD observed in [23, 24] static or transient?

An attempt is made to answer some of the above questions in the present communication. In § 2, the experimental set-up is briefly described; the experimental results on thresholds for different kinds of static PD, measurements on pretransitional biaxiality, the hysteresis width of transitions and detection of flow are also presented. Section 3 summarizes the main conclusions of this work and discusses directions for future investigations.

2. Experimental set-up and results

The experimental set-up is shown in figure 1 and was similar to that employed in ref. [23]. Thick cells were constructed using flat sheet electrodes made of stainless steel. The electrodes were annealed in a 900°C oven for several hours to get them as flat as possible; they were then washed with distilled water and acetone before constructing the cell. The glass plates were treated with a silane solution to ensure homeotropic alignment. Table 1 contains the dimensions of the cells used for the different experiments performed in this project. The construction of a variety of cells with different physical dimensions helps in the study of the scaling of thresholds. Sometimes, more than one cell had to be used in a given experiment, as the sample in a given cell deteriorated with time. The nematic liquid crystal used (EM Industries) had a nematic–isotropic transition of 35·5°C. The bulk ionic conductivity was expected to be 10^{-10} mho cm^{-1} according to the specifications of the manufacturer. Once a bottle of 5CB was opened, it was stored in a desiccator to prevent deterioration from moisture. The initial orientation $\mathbf{n}_0$ was along z which was also the direction of the stabilizing **H** field, while the electrodes were in the yz plane; a.c. voltage was measured and reported in rms volts.

Table 1. Dimensions of samples used.

Cell number	Thickness /μm	Electrode gap/mm	Figure reference
1	584	4·84	5 (*a–c*), 7
2	610	5·16	5 (*a*), 6
3	600	4·77	5 (*a*)
4	640	4·68	2 (*a, c, d*), 3 (*c, d*), 5 (*a–d*), 8
5	560	4·40	3 (*a, b*), 4, 5 (*a–c*)
6	417	4·05	5 (*a–d*)
7	530	4·13	5 (*d*)
8	200	5·15	9
9	600	4·65	2 (*b*)

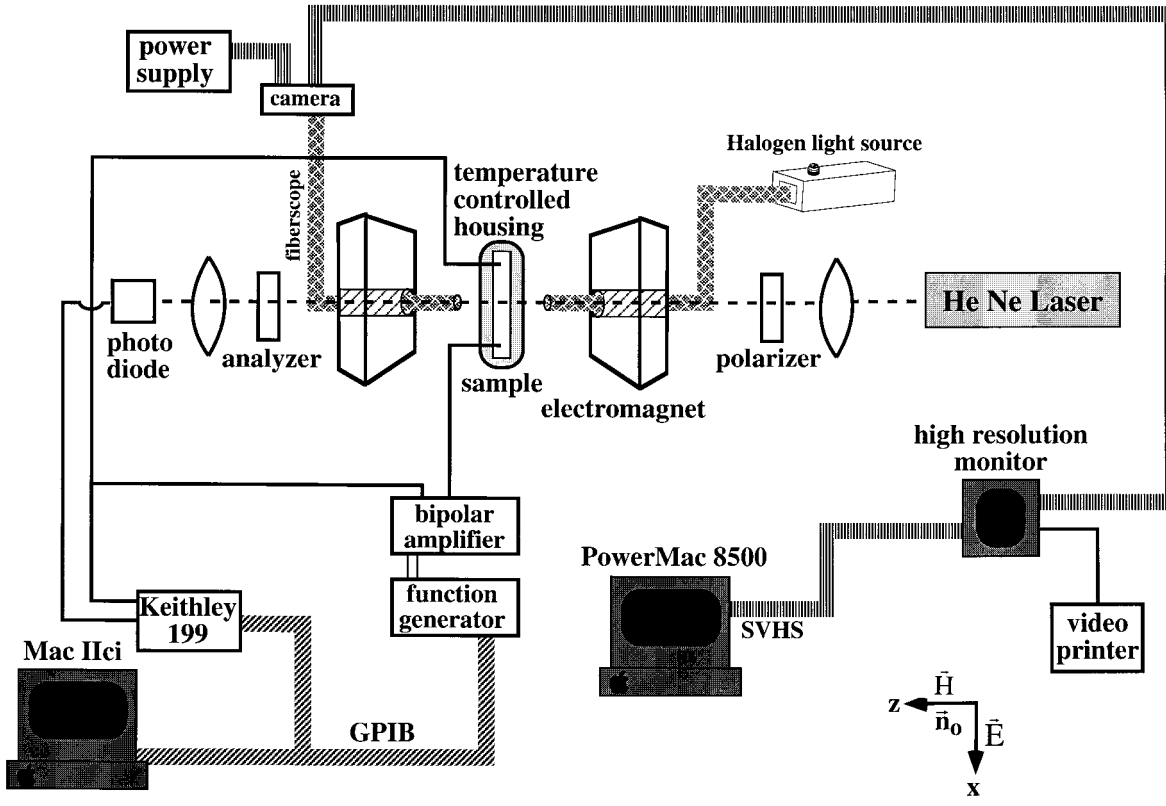

Figure 1. Experimental set-up. **E** = electric field, **H** = magnetic field, $\mathbf{n}_0$ = undistorted director.

The cell was housed in a thermostat which achieved long term temperature stability of better than ± 10 mK around a mean temperature of 28°C. Thresholds for the onset of orientational instabilities were optically monitored using the video technique described before [23]. Photovoltage measurements were also performed with light from a He–Ne laser incident along z on the centre of the sample.

The photodiode sensed orientational changes occurring over only a narrow region of the sample midway between the two electrodes. At a fixed **H** field, the voltage applied between the electrodes was ramped up from zero at a steady rate of $2{\cdot}3 \times 10^{-3}$ V s^{-1}; this is the ramp rate used for most of the measurements. With this ramp rate, deformations observed above thresholds were stationary if the voltage above the threshold value was held fixed. To calculate a threshold from photodiode data, line fits were made to the baseline and to the sharply rising portion of the curve. The voltage corresponding to the intersection of the two lines was taken to be the threshold. This is a consistent method for threshold determination by this technique. The imaging system was a fibrescope attached to a CCD video camera whose output was digitized by the video board on a Power Macintosh 8500. For the video observation of the striped phase, back lighting was employed. The lens used on the fibrescope, however, appeared to give slightly distorted images; for instance, the electrodes may appear curved as a consequence.

2.1. *Field induced biaxiality*

Observations were made to study this phenomenon in the present instance. Two different cases were studied. In the first, cell 4 was used. With **H** = 1000 G, the voltage was slowly increased at $f = 900$ Hz. The photodiode trace in the presence of crossed polarizers is shown in figure 2 (*a*). The intensity increases continuously, but slowly with voltage. When the voltage attains a sufficiently high value, the intensity rises sharply; this is referred to as the 'photodiode threshold' in the present work. Beyond the threshold, the intensity dips and then rises again to saturate at some value. Interestingly, no two photodiode runs (different **H** field and different frequency) behaved identically though most conformed to the description given above up to the rise at threshold. In a thick sample, even a small variation in the average director orientation could cause a considerable change in the path difference between the ordinary and extraordinary rays leading to oscillations in the transmitted intensity between crossed polarizers. Evidence of this is

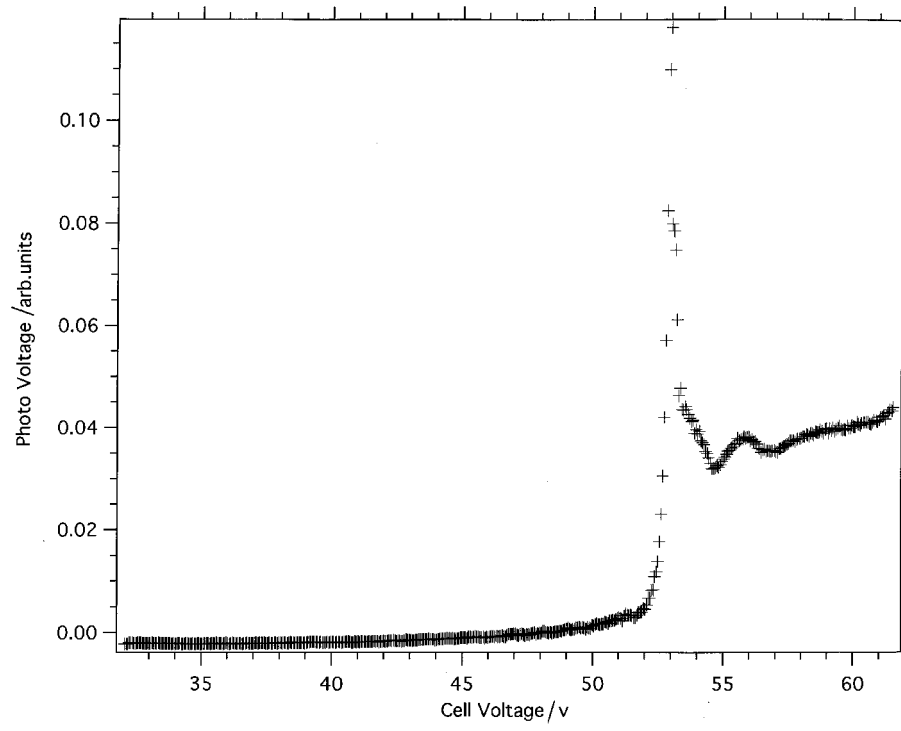

(*a*)

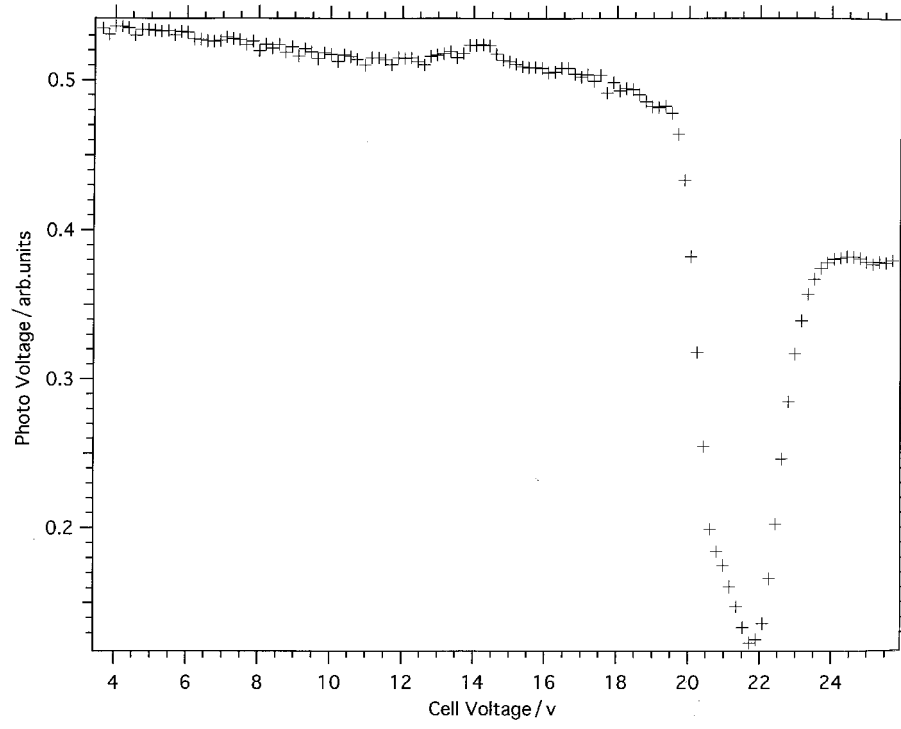

(*b*)

Figure 2. Sample photodiode traces for different magnetic strengths and frequency. The photodiode sensor is midway between the two electrodes; the photovoltage is measured in arbitrary units. (*a*) Between crossed polarizers, $H = 1000$ G, $f = 900$ Hz; the sharp increase of photovoltage indicates onset of deformation in the director field at the sample centre. (*b*) Without polarizers, no stabilizing magnetic field, d.c. voltage; the drop in transmitted intensity above transition is due to scattering by turbulent flow inside the sample. (*c*) Between crossed polarizers, $H = 0$, $f = 1500$ Hz; voltage ramp up. (*d*) Between crossed polarizes, $H = 0$, $f = 1500$ Hz; voltage ramp down. The hysteresis is clearly evident.

available in some cases; when the intensity rises after the dip, it oscillates about a mean value with further increase in voltage.

The initial rise in intensity with voltage is a clear indication of field induced pretransitional biaxiality [17]. The stabilizing **H** along z quenches uniformly the

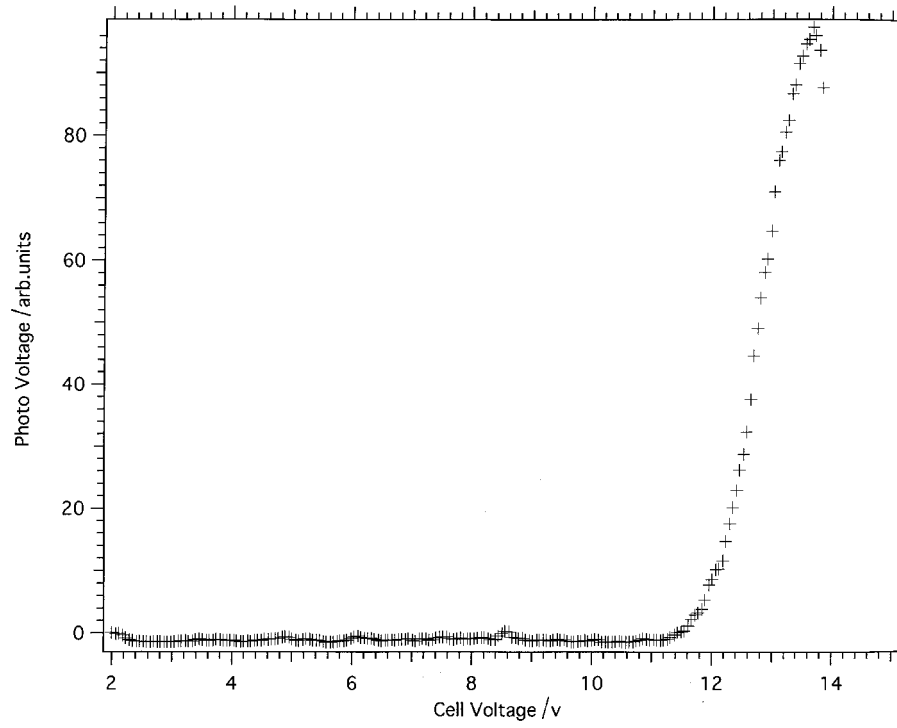

(*c*)

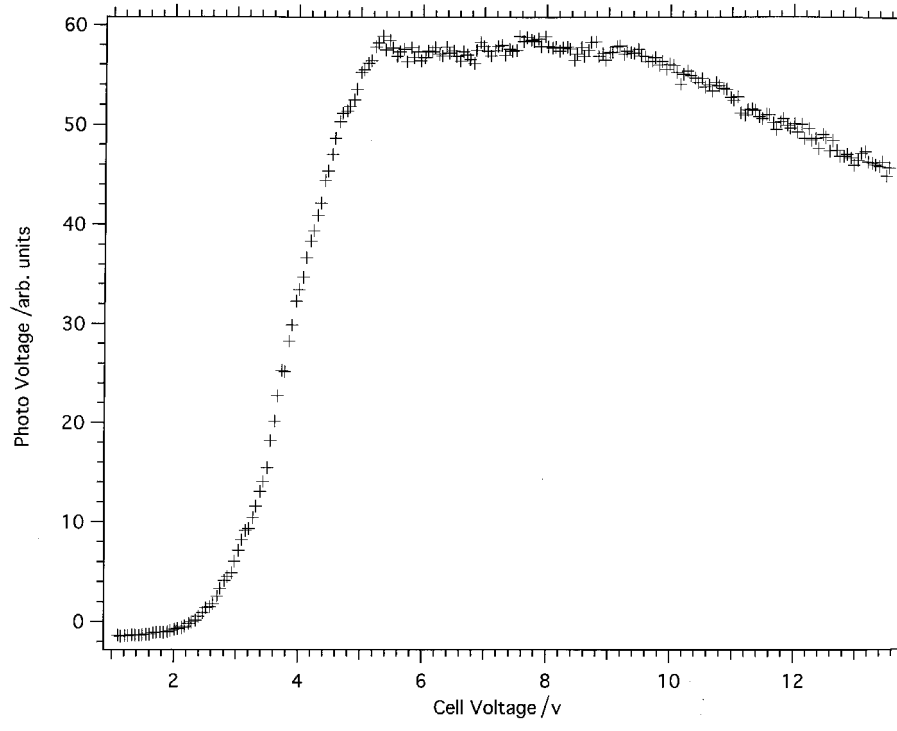

(*d*)

Figure 2. (*Cont.*)

director fluctuations that occur in every plane containing the z axis. If **H** is strong enough, the intensity of light transmitted along the optic axis (z axis) between crossed polarizers is negligible. Even in the presence of small director perturbations, the cylindrical symmetry about z is not lost. Once voltage is applied, the situation

changes: the destabilizing **E** along x has no effect on fluctuations in the yz plane but it enhances fluctuations occurring in other planes, its effect being maximum on fluctuations in the xz plane. This causes a small director deformation, with the x component stronger than the y component. Consequently, a small amount of light is transmitted through the crossed polarizers as the voltage is increased from zero [figure 2(*a*)]; the intensity shows a slow but steady growth with voltage. In other words, the uniaxiality of the sample about the z axis is broken and the sample effectively becomes optically biaxial; the degree of biaxiality grows with voltage.

The above mentioned observation is to be contrasted with the results of figure 2(*b*) for cell 9. These results are represented in anticipation of some effects which will be described later. In this case, **H** is switched off; the polarizers are also removed. In the absence of applied voltage, the light intensity transmitted is maximum. Now d.c. voltage is applied. As the voltage is increased, the intensity starts to diminish slowly; at a threshold, the photodiode output exhibits a sharp decrease and then an increase; at higher voltages, transmitted intensity diminishes and saturates at some lower value. It is found (see § 2.8) that the processes represented by figures 2(*a*) and 2(*b*) are entirely different. The results of figure 2 correspond to a region near the sample centre. A more complete understanding of the onset of director deformation results from optical observations reported in subsequent sections. It is now possible to view almost the entire sample and record thresholds for the onset of deformations even when these distortions develop away from the centre of the sample. As explained below, it is now possible to construct 'state diagrams' at different electrical frequencies.

2.2. *State diagram for the modulated phase*

State diagrams for different deformations were obtained in the V–B plane. A typical sequence of observations will first be described with emphasis on the high frequency regime. When the voltage is increased from zero at a fixed **H** field, a cloudy region appears near one of the electrodes. On further increase of voltage, a similar cloud starts to form near the other electrode. The first cloudy region is monitored as voltage is continuously enhanced; then, modulations appear inside the cloud near the electrode. Depending upon the strength of **H** and the frequency, the modulations may be along y [X stripes; figure 3(*a*)] or along x [Y stripes, figure 3(*c*)]. As soon as the stripes are resolved sufficiently to be identified as periodic, the voltage across the cell (e.g. V_M) is taken to be the threshold for the onset of the given PD. The voltage can be increased further to find out how the modulated phase evolves in other regions of the sample. At a voltage slightly higher than V_M, stripes are manifest in the second cloudy region near the other electrode. At a still higher voltage, the two banded regions travel towards the centre of the cell where they merge (or interfere) to result in static XY deformations [figure 3(*b*)], regardless of whether the stripes near the electrodes were initially X or Y. The XY deformations appear to form as a consequence of 'curling up' of the original X or Y stripes. When the voltage is ramped up further, the XY deformations grow fainter and start to disappear; finally, the cell becomes stripe-free. The sample appears dark between crossed polarizers showing that the director field is aligned along x in the bulk of the sample. The above scenario is typical of strong stabilizing magnetic strengths, $H > 1000$ G. For weaker H fields (see § 2.3), the initial modulated phase to be stabilized is XY.

Figure 4 contains the state diagram obtained with cell 5 at $f = 1500$ Hz. Six different **H** field strengths were chosen ranging from 1000 to 3000 G. As the stripes are diffuse for weak **H** fields, the range $H < 1000$ G was not included in figure 4. An increase of voltage at a given **H** leads to the formation of X stripes and then XY deformations; finally, the orientation in the sample appears to become aligned along x at a sufficiently high voltage. Values of the visually detected X threshold are available for five other cells (1–4 and 6; see table 1) which have different sample thicknesses as well as different electrode gaps. The existence or otherwise of the well-known scaling with respect to cell dimensions can now be ascertained through order of magnitude arguments connected with small deformations (remembering that the distortions reported by us are non-linear) in a sample limited along only one direction.

According to the continuum theory [1, 2], static instability thresholds are obtained by balancing elastic torques against destabilizing torques exerted by external fields. For small deformations, the elastic torque per unit volume is of the form $K(\mathrm{d}^2\theta/\mathrm{d}\alpha^2)$ where K is a curvature elastic constant, θ the (angular) deformation in **n** and α a coordinate (x, y or z) having the dimension of length. The electric and magnetic torque densities are given by $\varepsilon_A E^2/(4\pi)$ and $\chi_A H^2$, respectively, where H is the magnetic intensity. The equation of equilibrium requires that the sum of these torques vanish at all points in the sample. When the sample is limited only along z, α can be scaled by the semi-sample thickness (h) and the equation of equilibrium multiplied throughout by h^2. Then the electric and magnetic terms take the form $\varepsilon_A E^2 h^2/(4\pi)$ and $\chi_A h^2 H^2$, respectively. The products Eh and Hh occur together. For rigid anchoring of **n** at the boundaries, results for different sample thicknesses can be made identical by plotting the scaled electric potential Eh versus the scaled magnetic potential Hh.

In the present case, the cells are finite; in particular, the electrode gaps are different in different samples with

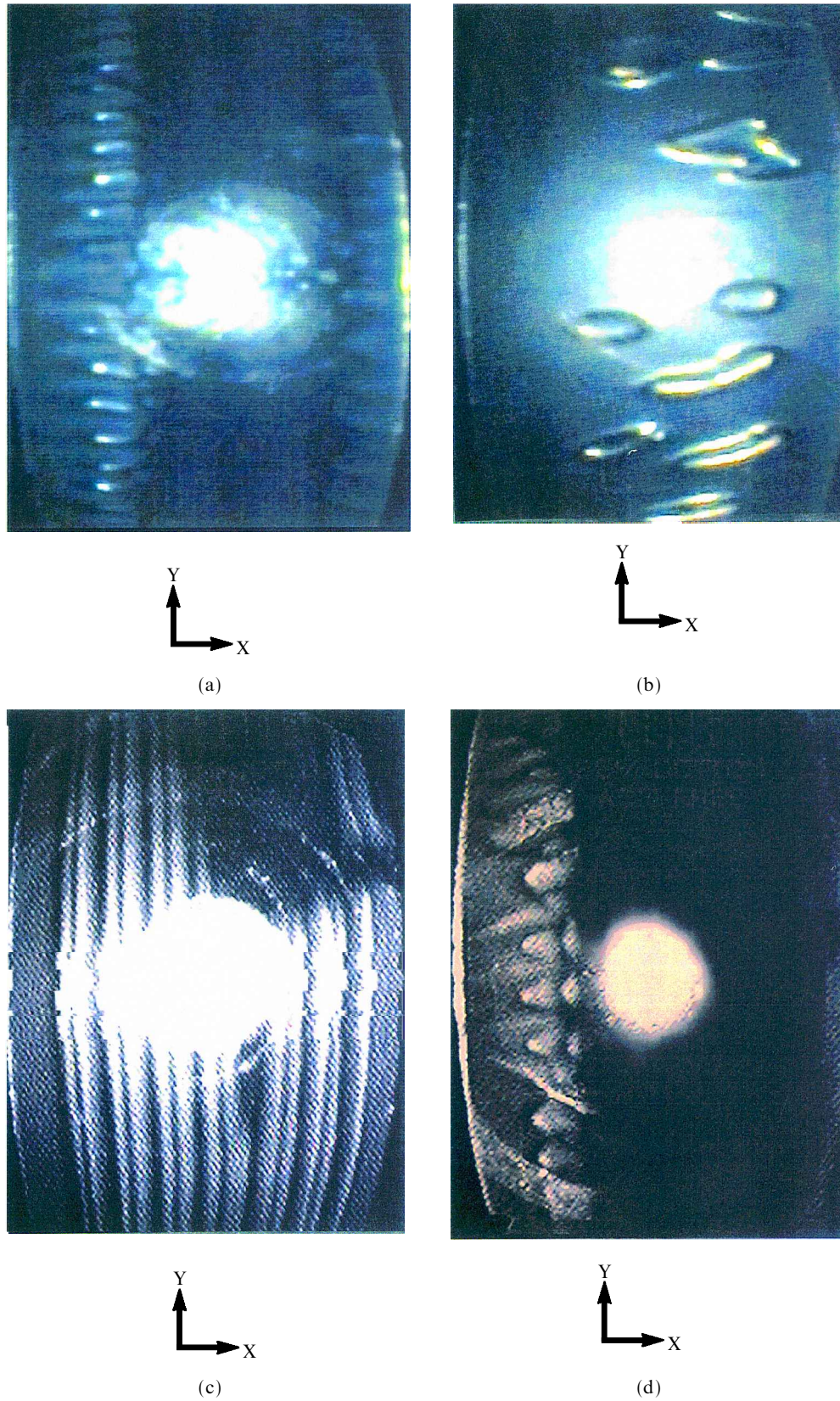

Figure 3. Appearance of the modulated phase of different kinds in cell 5 [figures 3 (*a*), and 3 (*b*)] and cell 4 [figures 3 (*c*), and 3 (*d*)] (see table 1). Voltage ramp rate $= 4{\cdot}5 \times 10^{-3}$ V s^{-1}; stabilizing magnetic field 1000 G for all cases. (*a*) *X* stripes, (*b*) *XY* deformations, (*c*) *Y* stripes, (*d*) $X+Y$ stripes. Frequency $f =$ (*a*) 1500 (*b*) 1500 (*c*) 30 (*d*) 600 Hz. Voltage $=$ (*a*) 44·63 (*b*) 50·82 (*c*) 51·71 (*d*) 46·89 V. The difference between the *XY* deformations and the $X+Y$ stripes may be noted. In (*a*), *X* stripes can be seen near one of the electrodes; (*b*) shows the *XY* deformations occupying the inter-electrode region.

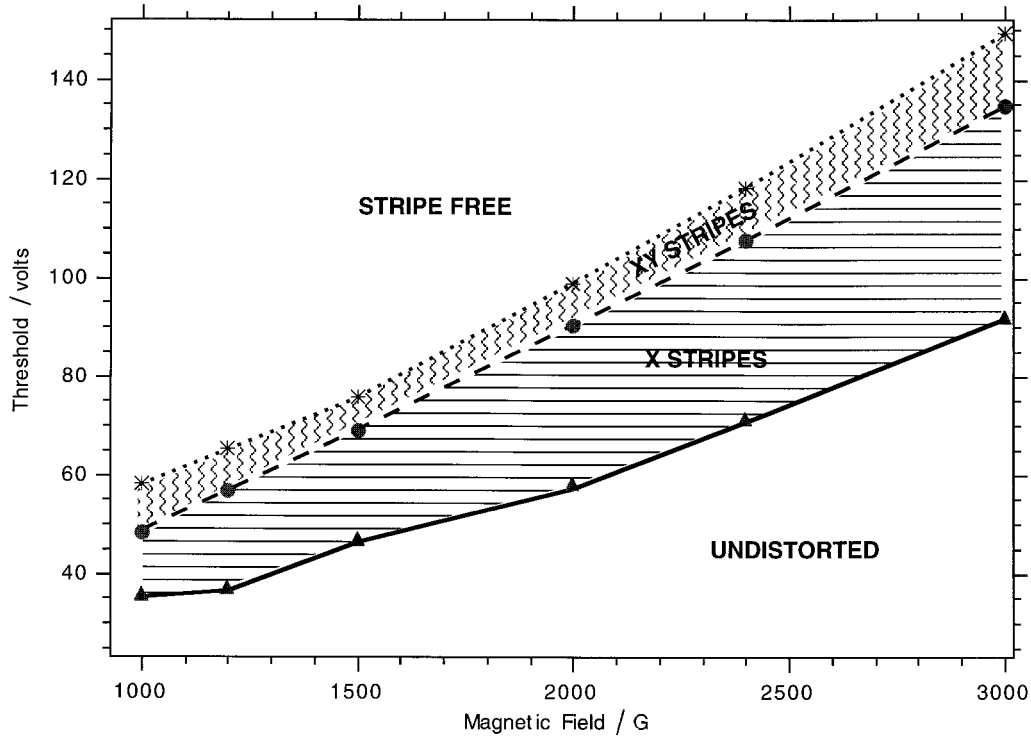

Figure 4. State diagram for the modulated phase at electric field frequency $f = 1500$ Hz for cell 5 at the ramp rate of $2{\cdot}3 \times 10^{-3}$ V s^{-1}. Triangles indicate the X threshold, circles the XY threshold and stars the stripe-free threshold. This diagram is complemented by figure 7.

$E = V_0/(2g)$ where $2g$ is the electrode gap and V_0 the applied voltage. The scaled electric potential is $V_0 h/g$. Scaling is tested by plotting the scaled X stripe threshold voltage $V_M h/g$ as a function of the scaled magnetic potential $2Bh$ for different cells at $f = 1500$ Hz [figure 5 (*a*)]. Points from different cells lie fairly close together showing that scaling exists for this threshold. Values for the other thresholds (X stripe to XY transition, XY to stripe-free transition at $f = 1500$ Hz; Y stripe at $f = 100$ Hz) have also been obtained for different cells and are shown in figures 5 (*b*)–5 (*d*). Scaling appears to hold for all these thresholds. The curves all seem to be linear in the range of **H** fields used. Results for weaker **H** fields have not been included due to the difficulty in locating the thresholds; it is likely that the variations of the electric threshold for weak **H** fields becomes non-linear (see, for instance, figure 1 of ref. [21] which represents theoretical calculations for linear perturbations). If this is true, then linear extrapolation of the curves in figure 5 to low **H** fields may lead to erroneous conclusions.

The voltage changes are dynamic, though slow. Hence, a doubt may arise whether the PD seen is a static deformation or a transient convective structure [25]. This is checked as follows. Once the X or XY deformations forms, the voltage is kept constant. Observations even after a gap of 12 h show that the stripes remain unchanged; hence the deformations seen here are indeed static. The fact that the cloudy region representing the initial instability appears at different voltages at the two electrodes under a.c. excitation shows that there exists some asymmetry in the sample itself. This can be established by reversing the connections of the cell. The cloudy regions appear at the two electrodes in the same sequence as earlier.

The photodiode measurements are used to establish an important fact. Figure 6 compared thresholds obtained by two different techniques for cell 2. One is the threshold found by visual observation for X stripes. The other is the threshold determined from a plot of photodiode output: this is the voltage at which the photodiode output shows a steep rise. The photodiode threshold is consistently higher than the visual threshold. The difference between the two thresholds shows that when a distortion appears near the electrodes, **n** near the sample centre is relatively undeformed. This is clearly due to the inherent spatial inhomogeneity of **E** in the present configuration.

The factors that may contribute towards making **E** spatially inhomogeneous can be identified. The sample corners represent interfaces between glass (isotropic dielectric), nematic (anisotropic dielectric) and metal

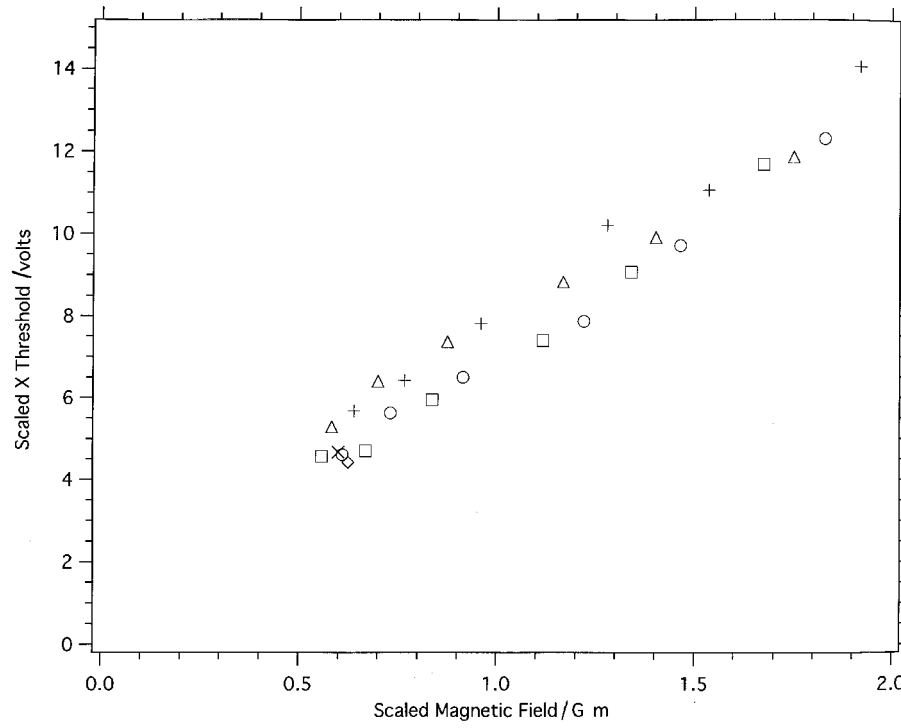

(*a*)

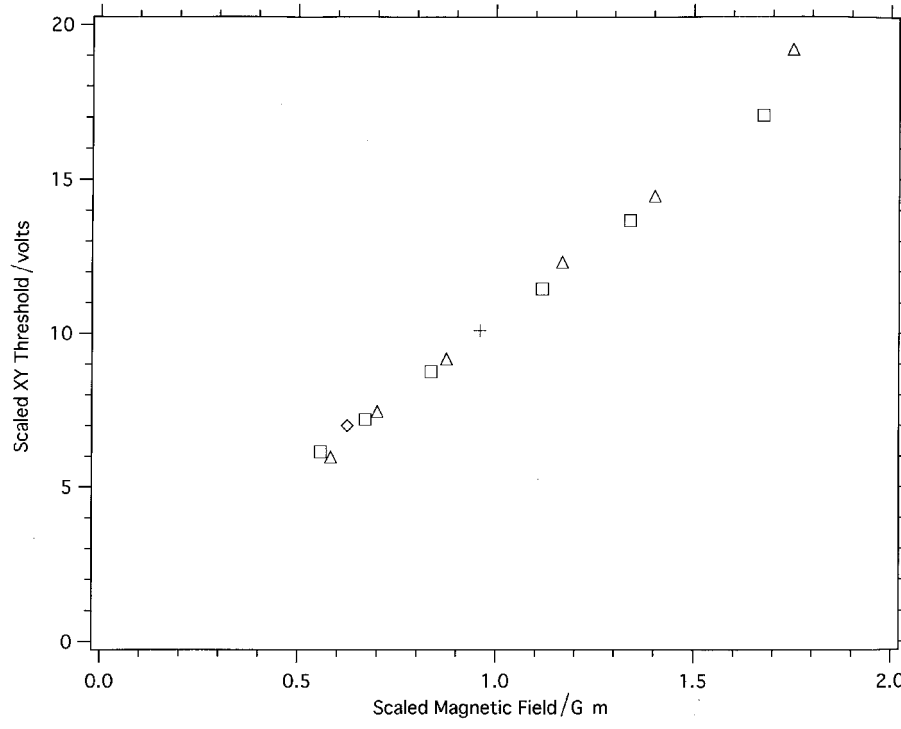

(*b*)

Figure 5. Plots of scaled threshold voltages versus scaled magnetic potential for $f = 1500$ Hz. (*a*) Scaled X threshold of cells 1 (open triangle), 2 (open circle), 3 (cross), 4 (plus), 5 (open square) and 6 (open diamond); scaling appears to hold for all the above thresholds. (*b*) Scaled XY threshold of cells 1, 4, 5 and 6. (*c*) Scaled stripe-free threshold of cells 1, 4, 5 and 6. (*d*) Plot for $f = 100$ Hz scaled Y threshold of cells 4, 6 and 7 (star).

(conductor). At such points, **E** can be expected to be spatially non-uniform at even low applied voltages; this may cause the sample corners to act as nucleation points for a thresholdless distortion. The glass plates are treated to impart homeotropic orientation, but the electrodes are untreated. The possibility exists that

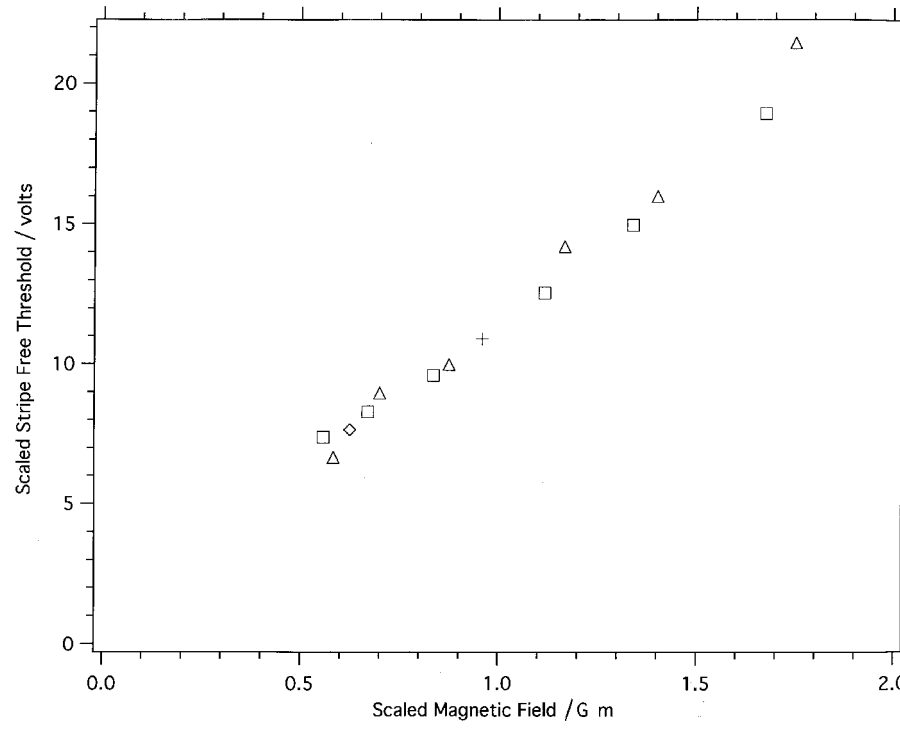

(*c*)

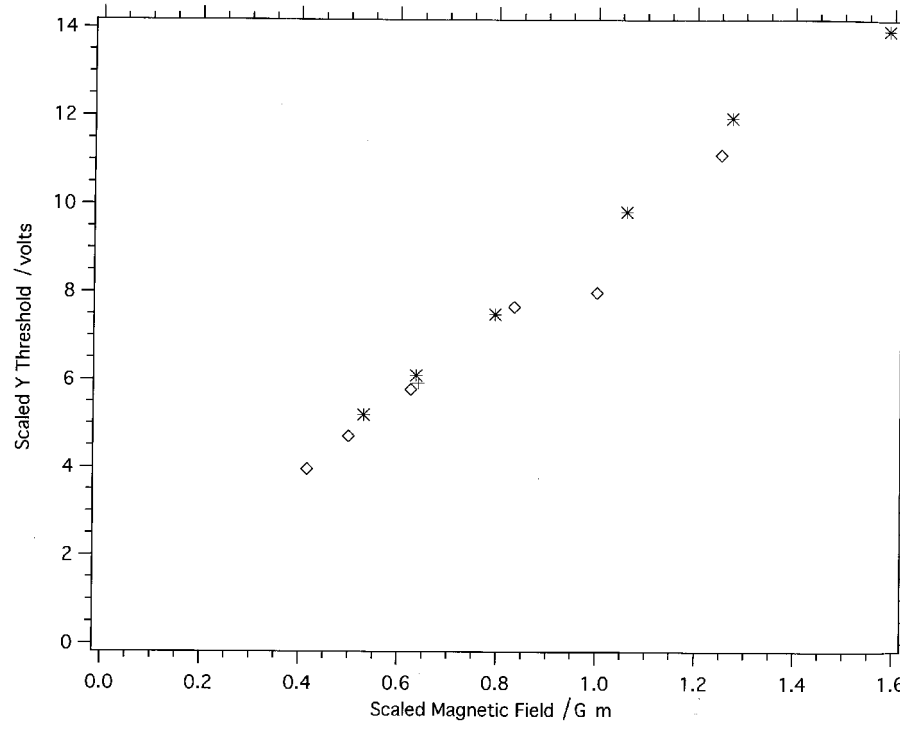

(*d*)

Figure 5. (*Cont.*)

even in the absence of voltage, the director field near the sample corners may contain defects. When the voltage is increased from zero, the already present distortion may grow with the voltage. We have not made a detailed optical search for defects near the sample corners.

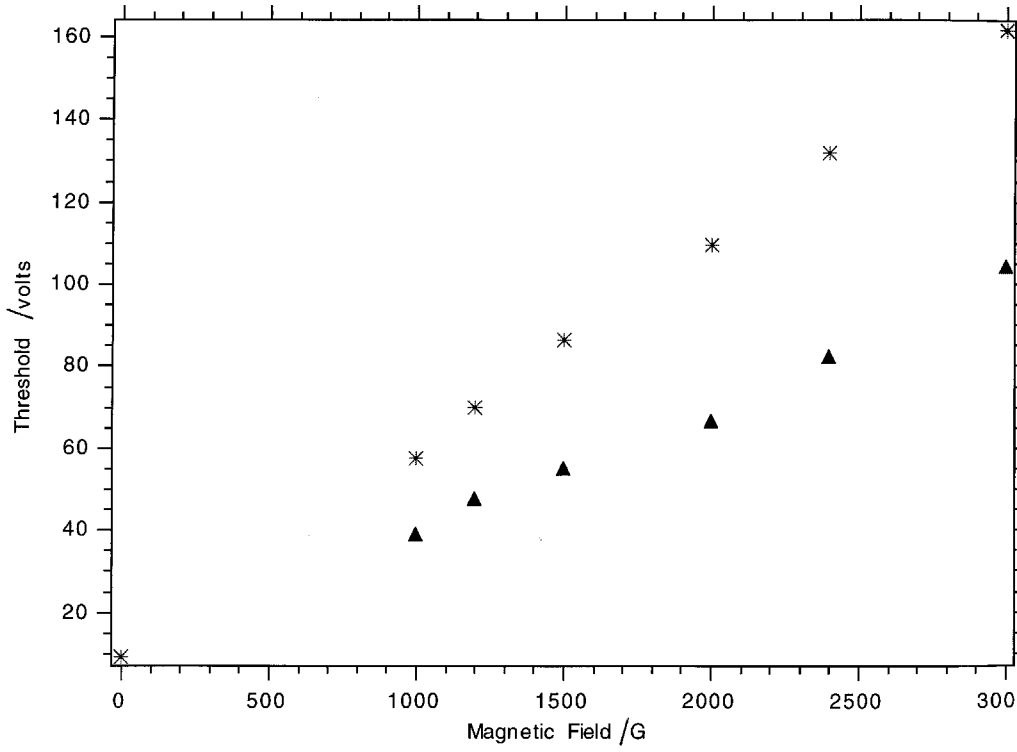

Figure 6. Comparison of experimental thresholds for cell 2 for onset of instability from the aligned state. At the given **H** field, the triangle represents the X threshold obtained from visual (video) observation. At the same **H** field, the star gives the only instability threshold that can be detected using the photodiode output. The star always lies above the triangle.

A limitation of photodiode measurements must be borne in mind. Visual observation reveals not only the transition from the initial aligned state to the X stripe, but also other transitions at higher voltage (from X to XY and then from XY to the stripe-free state). From the photovoltage measurement, the first transition is completely missed. Only the transition to XY distortions appears to be recorded as this occurs within the limited view of the photodiode sensor. At higher voltage, the change-over to the stripe-free state cannot be located at all, as the photovoltage simply saturates. During the transient movement of the stripes from the electrodes into the sample centre leading to the formation of the static XY deformations, the photovoltage does exhibit oscillations; this is clearly due to the temporal change in the average refractive index (or optical path difference) of the material. The remaining results of this work are based mainly on optical observations. In some places, the photodiode threshold is also included for comparison.

2.3. *Investigation of the cut-off* ***H*** *field*

Having found the phase diagram for strong **H** fields in the high frequency range, the weaker **H** field range is studied for the following reason. According to predictions of the linear perturbation model [21], the X stripes can set in above an electric threshold even without the stabilizing **H** field. The Y threshold does have a lower cut off **H** field, but being always less favourable than the X threshold, predictions for the Y stripes are of no real interest. It is, therefore, necessary to find out whether stripes can set in for weaker fields and in particular at $H = 0$.

Initially, f is fixed at 1500 Hz and **h** is constant. The voltage applied to the aligned sample is increased and the threshold, as well as the appearance of distortion above threshold, are visually monitored. Figure 7 captures the main results of observation at threshold. In the range $0 < H < 200$ G, it is not possible to see stripes or modulations. At transition, the initial alignment

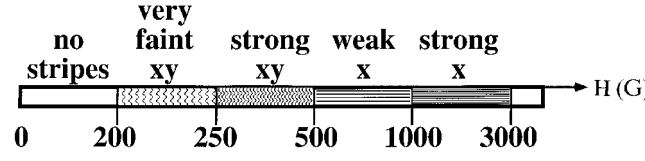

Figure 7. Qualitative phase diagram of the modulated phase as a function of H at $f = 1500$ Hz; H is known correct to ± 10 G. At low **H** fields, the transition appears to be to a homogeneous (aperiodic) deformation. These results are to be supplemented with those of figure 4.

appears to go over to HD with the distortion being uniform in the field of view†. Either stripes cannot appear or they are too diffuse to be seen. With increase in the voltage, the distortion remains homogeneous. At slightly higher H ($200 < H < 250$ G), faint XY deformations appear above a threshold voltage; these distortions also make their first appearance near the electrodes. When the voltage is increased further, they disappear leaving the sample stripe-free. In the next range ($250 < H < 500$ G), the XY deformations are again observed but they appear to be much less diffuse than in the lower B range. These again disappear from the cell at higher voltages leaving an aperiodic deformation. Finally, when $500 < H < 1000$ G, the post threshold deformation is X stripe; but the stripes are fainter than those seen in the higher H ranges. These fade away with increase in voltage as in the other cases.

It should be clear why only a qualitative study has been reported for the weaker **H** fields. As the stripes that appear are diffuse, it is difficult to pinpoint the threshold accurately. It is also difficult to measure the exact voltage at which the sample becomes stripe-free. Still, this investigation makes is possible to distinguish between three distinct ranges of **H** field. In the 'first range' studied in figure 7 ($0 < H < 200$ G), a single transition occurs from the initial aligned state to HD. In the 'second range' ($200 < H < 1000$ G), two transitions are observed—one from the initial aligned state to a stripe deformation (generally diffuse), the second from the stripe deformation to the aperiodic state. In the 'third range' ($1000 < H < 3000$ G), three transitions are observed—from the initially aligned state to localized X stripes, then to extensive XY deformations and finally to the homogeneous deformation.

2.4. *Hysteresis measurement*

Previous studies have shown [16, 17] that the electric bend transition, even in the absence of a stabilizing **H** field, is discontinuous; the accompanying hysteresis width appears to agree well with theoretical calculations. Both threshold and width increase with a stabilizing **H** field but the width appears to be about an order of magnitude less than the calculated value for strong **H**. Hence, hysteresis (if present) must be studied in the present case.

Hysteresis was measured for two different cases with a.c. frequency of 1500 Hz: (i) in the absence of **H** by photovoltage measurement at the sample centre; (ii) for the modulated phase with **H** of 1500 G by visual observation without the use of polarizers. Cell 4 was used with a ramp rate of $0{\cdot}013$ V s^{-1}.

The measurement of hysteresis width is straightforward. For case (ii), the voltage is increased from zero. Then, X stripes appear at $V(X)_{\rm th}$, say. On ramping up the voltage, XY deformations set in at a higher voltage, $V(XY)_{\rm th}$. On enhancing the voltage further, the sample becomes stripe-free at $V(\mathrm{SF})_{\rm th}$. The sequence is similar to the one described in figure 4; the voltage is increased above $V(\mathrm{SF})_{\rm th}$ and then diminished. Interestingly, XY deformations do not appear at all. The only modulated phase seen is the X stripe and it appears at $V'(\mathrm{SF})_{\rm th} > V(X)_{\rm th}$ but occupies almost the entire inter-electrode gap. When the voltage is decremented further, the cell becomes stripe-free at $V'(X)_{\rm th}$ but there exists uniform illumination (polarizers are not used for this particular measurement; presumably, the sample is close to the initial aligned state). The sequence of observations is summarized in table 2. The appearance of the XY deformations above the X stripe only during the voltage increase is somewhat intriguing. It appears that the transition from X to XY is 'monotropic' (assuming that increase of voltage is 'heating').

For case (i), the field of view is initially dark. Under voltage increase, $V_{\rm th}$ is the point at which the photovoltage starts increasing sharply [figure 2(*c*)]; under further increase of voltage, the photodiode output saturates. When voltage is diminished, the photovoltage starts decreasing sharply at $V'_{\rm th}$ [figure 2(*d*) and table 2]. The question mark against HD in table 2 appears because the deformation is not strictly homogeneous. By definition, HD should be uniform in the sample plane and is expected to occur at the same threshold in all parts of the sample. Visual observation reveals that the distortion starts (in the form of a cloud) near either electrode and spreads to the centre above the photodiode threshold causing a dark line (like a wall) to appear midway between the electrodes. At this stage, the sample appears to be stripe-free on either side of the line.

2.5. *Frequency dependence of threshold at* $\boldsymbol{H = 0}$

The effect of frequency on the onset of instability was studied in the absence of **H** (figure 3 of ref. [24]). Cells 1 and 2 were used for this study and the thresholds were

Table 2. Hysteresis data.

H Gauss	Deformation	Ramp up $V_{\rm th}$/V	Ramp down $V'_{\rm th}$/V	Hysteresis width/V
0	HD(?)	12·07	5·35	6·72
1500	X stripe	57·10	55·39	1·71
1500	Stripe-free	84·57	78·94	5·63

† Formally, HD is a director distortion that is uniform in the sample plane. We refer to the post threshold deformation as HD if stripes are not seen. Though stripes are absent, HD observed by us will not be uniform especially near the electrodes.

determined only for ramp up. The voltage at which the photovoltage starts rising sharply was taken to be the threshold. For a given cell, the threshold remains more or less constant in the higher frequency range. When the frequency diminishes to around 200 Hz, the threshold also deceases. For $f < 150$ Hz, the threshold drop is very sharp; there is a strong indication that for d.c. excitation, the threshold may be either very small or even zero. The dielectric constants of the material are known to be almost independent of the frequency for $f < 1500$ Hz [15]. Based on the qualitative discussion in § 1, the following points can be stated.

(i) Theoretical analysis shows [12] that the calculated threshold for the onset of instability becomes frequency dependent even when the individual conductivities are assumed to be independent. This frequency dependence stems from the time varying nature of **E**. This is one of the causes of frequency dependent thresholds in the present work.

(ii) The individual electrical conductivities of a nematic are themselves known to vary with the frequency of the applied field in some materials, especially in the low frequency range ([26]; see also figure 2.8 of ref. [2]).

(iii) The steep droop in the threshold starting at about $f = 150$ Hz makes it possible to compare this frequency with a cutoff frequency via a simple calculation. It is well known [12] that for a nematic with planar alignment, a cutoff frequency is defined as $f_C = 4\pi\sigma_\perp/\varepsilon_\perp$ where $\sigma_\perp$ and $\varepsilon_\perp$ are, respectively, the electrical conductivity and the dielectric constant normal to the director. For homeotropic alignment, one similarly obtains $f_C = 4\pi\sigma_\parallel/\varepsilon_\parallel$ where $\sigma_\parallel$ and $\varepsilon_\parallel$ are quantities measured parallel to the nematic director. Taking $f_C = 150$ Hz and $\varepsilon_\parallel = 17{\cdot}86$ (from ref. [15]), the conductivity can be calculated. One obtains $\sigma_\parallel = 210\ \text{sec}^{-1} = 2{\cdot}34\ 10^{-8}$ mho m^{-1}. The actual values of electrical conductivities of the studied samples are not known. According to literature [2], it is not uncommon to find bulk conductivities $\sim 10^{-7}$–10^{-10} mho cm^{-1} in commercially available nematics.

(iv) Charge injection may also become important at low frequencies in the presence of conducting impurities. Indirect evidence for this is presented in § 2.7.

2.6. *Frequency dependence of stripe threshold*

The study reported in § 2.5 indicates that the photodiode threshold is strongly frequency dependent in the absence of a stabilizing **H**. It is possible that the stripe threshold is also a function of frequency in the presence of **H**; the direction of stripes may also become frequency dependent. This is tested as follows. **H** applied to the aligned sample is initially fixed at a high value (3000 G). The frequency is also fixed at the upper limit (1500 Hz). The voltage is increased from zero and the stripe threshold is visually determined as described earlier. In these experiments, the voltage is not greatly increased (i.e. about 10% of the threshold) above the first stripe threshold; the quantities of interest are the first threshold encountered and the nature of the stripes that are seen at and slightly above this threshold. Keeping H fixed, the experiment is repeated at other frequencies (down to 30 Hz). Then, H is decremented and the entire process repeated. The stripe threshold decreases with H at a given frequency. But an additional fact also emerges from a study of the frequency dependence of the stripe threshold at a fixed H.

Figure 8 contains the plots of stripe threshold (determined visually) and photodiode threshold as functions of frequency at $H = 1000$ G in the range $30 < f < 1500$ Hz. In general, the photodiode threshold is higher than the visual threshold for all frequencies; the two become close only in the low frequency limit. Three frequency ranges can be distinguished.

(i) The high frequency range, $900 < f < 1500$ Hz. Only X stripes are observed at and slightly above threshold. The appearance of the deformation is a set of bright and dark lines parallel to x; the brightness of a bright band is approximately uniform within that band. The X threshold decreases slightly with frequency in this range.

(ii) The middle frequency range, $300 < f < 900$ Hz. X stripes are seen at the first threshold. These appear again as uniform dark and bright stripes directed along x. The X threshold tends to increase slowly as the frequency is decreased. At the same time, the X stripes that form at threshold become more and more diffuse. (For $f < 300$ Hz, X stripes do not form at all.) In the middle frequency range, a new deformation appears above a well defined, second threshold when voltage is increased at a given frequency; we refer to this as the $X + Y$ stripes. As seen from figure 8, the $X + Y$ threshold is slightly above the X threshold. The resulting deformation appears to have a mixture of the X and the Y stripes; an example of the $X + Y$ stripe is shown in figure 3 (d). An approximate description of this deformation is that the X stripe remains but appears to become twisted so that the brightness of a bright stripe varies along the stripe. This distortion is to be distinguished from the XY

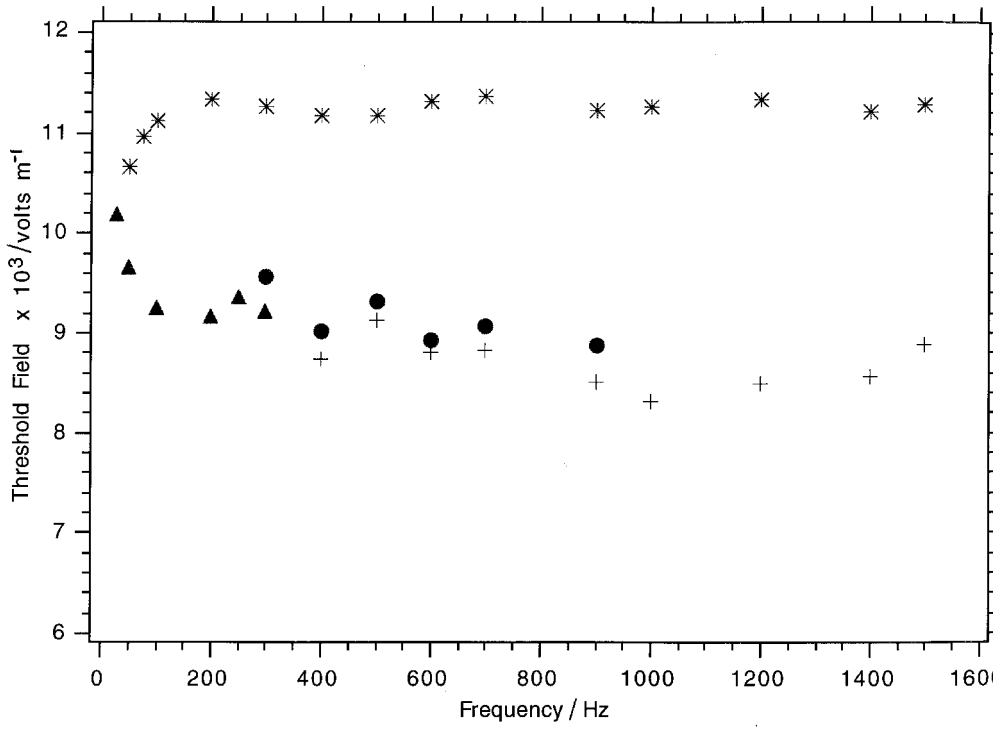

Figure 8. Variation of stripe threshold with the electric frequency at a fixed magnetic stength ($H = 1000$ G) for cell 4. The threshold is the first encountered when the voltage is increased from zero. Stars = thresholds from photovoltage measurements at sample centre; pluses = video observation of X threshold; circles = $X + Y$ threshold; triangles = Y threshold.

deformations encountered earlier [figures 3(*b*) and 4] in the high frequency range at high voltages; the direction of the XY deformations is itself inclined at some angle with the x axis.

(iii) The low frequency range, $30 < f < 300$ Hz. The deformation that appears at and slightly above threshold is Y stripe; X stripes or $X + Y$ stripes are not seen. The Y threshold rises rapidly as the frequency is diminished towards the lower limit.

2.7. *d.c. Thresholds*

The observations for a.c. excitation were generally repeatable, with qualitatively similar results being obtained in different cells. The effects of d.c., on the other hand, showed an erratic trend; observations in one cell not always being reproducible in another. While all reasons for this are not yet apparent, one possibility is the use of metal surfaces for electrodes [3]. A separate cell (with 600 μm thickness and 4·32 mm electrode gap) was used in these experiments. With a stabilizing **H** impressed on an aligned sample, video observations and photovoltage measurements were separately performed as the voltage was increased from zero. For $H < 1200$ G, no modulated phase can be detected. Study of the photovoltage reveals that for weak **H** fields, the transmitted intensity increases continuously with voltage and saturates; hence there is no detectable threshold. This is consistent with the findings reported in §2.5 (sharp decrease of photodiode threshold in the low frequency range, though in another sample). For $H > 1200$ G, however, the distortion above threshold is of the XY type.

As has been already mentioned, the case of d.c. and low frequency fields is often complicated by the presence of other mechanisms, such as unipolar charge injection. Methods for demonstrating the existence of such an effect include reversal of the polarity of the cell and the use of a.c. excitation. This was done for cell 4 with $H = 1500$ G. With a frequency of 1500 Hz, the voltage was ramped up until a cloudy region was observed near one electrode (say, the right electrode). For the same cell with d.c. excitation, the cloud starts to appear first at the other electrode (left); the situation does not change when the d.c. polarity is reversed. This difference between a.c. and d.c. excitations appears to indicate that processes of an electrochemical type may be active under d.c. excitation.

2.8. *Detection of EHDI*

The frequency dependence of the thresholds (figure 8) has already shown that the instability mechanism should involve electrical conductivity of the medium.

Interestingly, the shape of the threshold versus f plots in our $H = 0$ data [24] is qualitatively similar to that of the conductivity versus frequency curves for some nematics ([26]; figure 2.8 of ref. [2]). A fact that strengthens this conclusion is the observation of threshold for weak **H** fields at high frequency and the non-existence of a d.c. electric threshold. It is quite possible that effects of conductivity are weakened at higher electric frequencies. This makes it necessary to look for hydrodynamic flow under d.c. excitation as this is the signature of EHDI.

To test for the presence of flow effects, a cell (600 μm thick and 4·37 mm electrode gap) was constructed and filled with the nematic liquid crystal doped with a small quantity (approximately one hundredth by volume) of fine chalk dust. It is possible to obtain aligned samples even after mixing the impurity. The sample is left under a **H** field of 1000 G for some time; then, the voltage is increased until Y stripes appear. The voltage is increased slightly further and then kept fixed. When the cell is monitored through the video camera, particles are seen to come into and go out of view when the line of sight is directed along the z axis confirming cellular flow in the xz plane. Due to experimental limitations, it is not possible to make observations to decide whether or not there exists cellular flow in the yz plane also. When the voltage is kept fixed, the cellular flow continues indefinitely. The flow also appears to be stationary; the specks appear and disappear with reasonable periodicity. For a.c. excitation with $f = 1000$ Hz, the stripes appear but it is not possible to detect cellular flow.

A thinner sample (cell 8) was used for making microscopic observations. At zero **H** field and a frequency of 5 Hz, the voltage was raised. Figure 9 is a photograph of the sample just above threshold. Visual observation under crossed polarizers shows that the field of view is filled with fluctuating domains indicating turbulent flow with **n** changing continuously in a random way. In this state, the sample scatters light strongly. When light from the laser is shone on the sample and the sample viewed from a direction close to that of incidence, the surface of the cell appears to glow strongly. On moving the line of sight away from the direction of incidence, the glow diminishes. Observation of transmitted light from the other side of the cell shows a 'speckle' effect. Figure 2 (*b*) is the representative photodiode run (without polarizers) which gives a more quantitative confirmation of dynamic scattering.

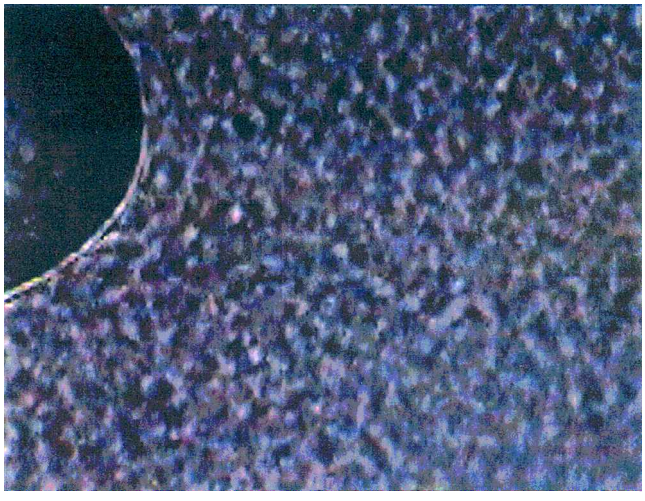

Figure 9. Microscopic observation of turbulence in cell 8 at zero **H** field, electric frequency of 5 Hz and a voltage of 74·64 V just above threshold [see also, figure 2 (*b*)]. The scale is 1 : 250. The picture shows a region to the top left which has not yet undergone the transition.

3. Conclusions

A nematic liquid crystal with initial homeotropic alignment has been subjected to crossed **H** and **E** fields, with **E** in the sample plane. Sample cells with different spatial dimensions were employed. In the absence of the stabilizing **H**, PD is not observed under a.c. excitation. When a.c. voltage is increased in the presence of a sufficiently strong **H**, more than one transition occurs leading to the formation of different types of PD. These transitions are evident from visual observation, and the observed PD does not appear to involve macroscopic flow. The thresholds conform approximately to a simple form of scaling. At sufficiently high voltages the stripes disappear. Repeated trials in a given cell result in the observation of the same sequence of transitions. Every transition between successive distortion states is discontinuous and is accompanied by hysteresis. The width of hysteresis is a small fraction of the threshold even when **H** is strong. The initial appearance of stripes only near the electrodes appears to indicate the presence of strong inhomogeneity close to the electrodes in the ground state director field and also in **E**. The nature of PD as well as the PD threshold show marked dependence on the frequency, especially when frequency is low. This seems to point towards the involvement of electrical conductivity in the instability mechanism. With d.c. excitation, convective flow is observed in the presence of a strong **H** field. Without the stabilizing **H**, turbulent flow (dynamic scattering) occurs. The bulk of observations have been made visually due to the limitation of the photodiode output described in the earlier sections. Some avenues that are open for future experiments are discussed below.

The results reported here pertain to a single temperature. This must be viewed in the light of temperature dependence of material properties. The present work does not report the stripe width of PD, but the general trend of increasing stripe width with diminishing H is observed. Accurate measurement of periodicity will be

attempted in the future. A detailed investigation of threshold scaling for different frequencies and magnetic fields is also called for. Due to the inhomogeneous distortion in the ground state with increase of voltage from zero, the magnitude of pretransitional biaxiality may be dependent on the point of observation. The photodiode is useful for the purposes of this study. In this work, the electrode surfaces are not coated with surfactants that impart specific director alignment. It should be possible to treat the electrodes suitably (to produce homogeneous alignment along z) to ensure better anchoring of the director at the electrodes. The use of surfactant may also regulate charge injection especially at low frequencies. The principal conductivities of the material are not known at present. The determination of these quantities as functions of the frequencies should shed more light on the frequency dependence of the thresholds. A similar trend can be expected for the variation of hysteresis widths. At present, we do not have sufficient data to discern a pattern in the variation of hysteresis width with different parameters.

A systematic study of effects of **H** on turbulence should prove interesting. We find that turbulence sets in at a low frequency when $H = 0$. This indicates a cutoff frequency above which turbulence may not occur at threshold even without a magnetic field. After turbulence sets in at $H = 0$, it may be possible to quench it by a gradual increase in H keeping the voltage fixed. It is not known at present whether such an increase of H will lead to different transitions (for instance, turbulent flow to steady state convective flow, convective flow to static homogeneous deformation).

When the director configuration changes beyond a threshold, the new configuration sets in only after an interval of time which depends upon the sample thickness, the field strengths, the material parameters, etc. By the time the new configuration is detected, the voltage would have changed in our experiment as the voltage changes are dynamic. This is the reason for keeping the voltage ramp rate as low as possible. Suppose the voltage is being increased from zero. If the ramp rate is considerably higher than $2{\cdot}3\,10^{-3}\,\mathrm{V\,s^{-1}}$, the threshold recorded by us are generally higher. When the voltage ramp up rate is high enough, transient PD is known to occur in a related configuration [23]. This underlies the importance of making a detailed study of the observed phenomena for different ramping rates. In a way, this will serve to generalize the usual experiment for observing transient periodic dissipative structures by the sudden application of a destabilizing field.

The authors thank a referee for useful comments on an earlier version of this work. S. Wild and B. Zurn acknowledge support provided by the National Science Foundation through an REU Grant DMR-9322301. We are grateful to Erica Bramley for her contribution to the turbulence data. S. Garg thanks the Luce Foundation for a grant administered by the College of Wooster, and the National Science Foundation for Grant No. DMR-8921719.

References

[1] De Gennes, P. G., and Prost, J., 1993, *The Physics of Liquid Crystals* (Oxford: Clarendon Press); Chandrasekhar, S., 1992, *Liquid Crystals* (Cambridge: Cambridge University Press).

[2] Blinov, L. M., and Chigrinov, V. G., 1993, *Electrooptic Effects in Liquid Crystal Materials* (New York: Springer-Verlag).

[3] Cognard, J., 1982, *Mol. Cryst. liq. Cryst. Suppl.*, **1,** 1; Jerome, B., 1991, *Rep. Progr. Phys.*, **54,** 391.

[4] Lonberg, F., and Meyer, R. B., 1985, *Phys. Rev. Lett.*, **55,** 718.

[5] Gooden, C., Mahmood, R., Brisbin, A., Baldwin, A., Johnson, D. L., and Neubert, M. E., 1985, *Phys. Rev. Lett.*, **54,** 1035; Garg, S., Crandall, K. A., and Khan, A. A., 1993, *Phys. Rev. E*, **48,** 1123.

[6] Allender, D. W., Hornreich, R. M., and Johnson, D. L., 1989, *Phys. Rev. Lett.*, **59,** 2654.

[7] Meyer, R. B., 1969, *Phys. Rev. Lett.*, **22,** 918.

[8] Deuling, H. J., 1978, *Solid State Phys. Suppl.*, **14,** 77.

[9] Dozov, I., Barbero, G., Palierne, J. F., and Durand, G., 1986, *Europhys. Lett.*, **1,** 563.

[10] Vistin, L. K., 1970, *Kristallografiya*, **15,** 594; Barnik, M. I., Blinov, L. M., Trufanov, A. N., and Umansky, B. A., 1977, *Zh. Eksper. Teoret. Fiz.*, **73,** 1936; Bobylev, Yu. P., Chigrinov, V. G., and Pikin, S. A., 1979, *J. de Physique (Paris)*, **40,** Colloq. C3, C3-331.

[11] Carr, E. F., 1969, *Mol. Cryst. liq. Cryst.*, **7,** 253; Helfrich, W., 1969, *J. Chem. Phys.*, **51,** 4092.

[12] Orsay Liquid Crystal Group, 1971, *Mol. Cryst. liq. Cryst.*, **12,** 251; Dubois-Violette, E., de Gennes, P. G., and Parodi, O., 1971, *J. de Physique*, **32,** 305.

[13] Hirakawa, K., and Kai, S., 1977, *Mol. Cryst. liq. Cryst.*, **40,** 261.

[14] Carr, E. F., Ackroyd, P. H., and Newell, J. K., 1977, *Mol. Cryst. liq. Cryst.*, **43,** 93; Carr, E. F., and McClymer, J. P., 1990, *Mol. Cryst. liq. Cryst.*, **182B,** 245; Carr, E. F., 1991, *Mol. Cryst. liq. Cryst.*, **202,** 1, and references therein.

[15] Cummins, P. G., Dunmur, D. A., and Laidler, D. A., 1975, *Mol. Cryst. liq. Cryst.*, **30,** 109.

[16] Frisken, B. J., and Palffy-Muhoray, P., 1989, *Phys. Rev. A*, **39,** 1513.

[17] Frisken, B. J., and Palffy-Muhoray, P., 1989, *Liq. Cryst.*, **5,** 623.

[18] Arakelyan, S. M., Karayan, A. S., and Chilingaryan, Y. S., 1984, *Sov. Phys. Doklady*, **29,** 202.

[19] Seppen, A., Maret, G., Jansen, A. G. M., Wyder, P., Janssen, J. J. M., and De Jeu, W. H., 1986, *Springer Proc. Phys.*, **11,** 18; Dunmar, D. A., Szumilin, K., and Waterworth, T. F., 1987, *Mol. Cryst. liq. Cryst.*, **149,** 385.

[20] Allender, D. W., Frisken, B. J., and Palffy-Muhoray, P., 1989, *Liq. Cryst.*, **5,** 735.

[21] KINI, U. D., 1990, *J. de Physique (Paris)*, **51,** 529.
[22] SCHELL, K. T., and PORTER, R. S., 1989, *Mol. Cryst. liq. Cryst*., **174,** 141.
[23] GARG, S., SAEED, S., and KINI, U. D., 1995, *Phys. Rev. E*, **51,** 5846.
[24] GARG, S., SAEED, S., WILD, S., BRAMLEY, E., and KINI, U. D., 1997, *Mol. Cryst. liq. Cryst*., **302,** 379.
[25] CARR, E. F., 1977, *Mol. Cryst. liq. Cryst*., **34,** L 159; GUYON, E., MEYER, R. B., SALAN, J., 1979, *Mol. Cryst. liq. Cryst*., **54,** 261; for a review, see SRAJER, G., FRADEN, S., and MEYER, R. B., 1989, *Phys. Rev. A*, **39,** 4828.
[26] SCHADT, M., and VON PLANTA, C., 1975, *J. chem. Phys*., **63,** 4379.